Earth and Planetary Science Letters 433 (2016) 44–53

Contents lists available at ScienceDirect

Earth and Planetary Science Letters

www.elsevier.com/locate/epsl

On the slow decompressive response of volatile- and crystal-bearing magmas: An analogue experimental investigation

Laura Spina *, Corrado Cimarelli, Bettina Scheu, Danilo Di Genova, Donald B. Dingwell

Department für Geo- und Umweltwissenschaften, Ludwig-Maximilians-Universität München, Theresienstrasse 41, 80333 Munich, Germany

ARTICLE INFO

Article history:
Received 11 June 2015
Received in revised form 18 October 2015
Accepted 19 October 2015
Available online 2 November 2015
Editor: T.A. Mather

Keywords:
decompression
bubbly fluid
magma analogue
foam
nucleation

ABSTRACT

The degassing kinetics of ascending magma strongly affect eruption dynamics. The kinetics are in turn influenced by magma properties. The investigation of the relationship between magma properties and eruption dynamics is a key element in revealing the processes characterizing magmatic flows within the shallow conduit. To explore the effects of physical properties on degassing in basaltic eruptive systems, we have designed and carried out experiments on the slow decompressive response of analogue magmas, composed of silicone-oil-based suspensions, using a shock-tube apparatus. Four series of experiments were performed: 1) particle-free silicone oils with viscosity ranging from 1 to 1000 Pa s were used to constrain the liquid response; 2) silicone oils with variable proportion of suspended micrometric spherical particles were employed to assess the effect of different crystal fractions; 3) suspensions of elongated particles in silicone oils were used to investigate the role of crystal shape; 4) the effects of saturation time and pressure were examined. The rheology of both spherical- and elongated-particle-bearing suspensions were characterized by concentric cylinder rotational rheometry. The flow dynamics of the bubbly fluid, from the process of bubble nucleation up to the development of a permeable bubble network, were constrained using image analysis. Different fluid regimes were distinguished: (i) nucleation, (ii) foam build-up and (iii) foam oscillation. By comparing results obtained from the different series of experiments, we were able to assess the primary role played by the presence of particles on the evolution of the gas volume fraction within the samples. Particle fraction has a dominant role at high concentration, affecting the motion of the fluid. Finally, particle shape influences the long-term degassing efficiency of the fluid. Using scaling considerations, such observations are applied to mafic to intermediate systems. The results of our experimental investigation contribute to constraining vesiculation processes in magmas of various crystallinities at shallow depths.

1. Introduction

The physical processes occurring within a volcanic system are manifold. The phenomena and products observed at the surface result from dynamic shifts in magmatic properties during ascent. Amongst these processes, volatile exsolution plays the fundamental role of generating the added buoyancy, which is the main driving force of ascent. Moreover, degassing can drive crystallization with dramatic rheological consequences (Chevrel et al., 2015). Clearly, degassing kinetics are at the centre of many eruption dynamics. One example is the intimate link between the traces of degassing in eruptive products and the pressure state of the system, highlighted by Toramaru (2006), utilising bubble number density as a proxy for decompression rate.

The nucleation and growth of bubbles during decompression has been the focus of several studies. Sparks (1978), for instance, analytically investigated the diffusive and decompressional growth rate of a bubble in an infinite melt reservoir. Later, Proussevitch et al. (1993) included the effect of melt advection due to bubble growth. Barclay et al. (1995) modeled the instantaneous decompression in high viscosity magma of either a single bubble surrounded by an infinite melt or a thin shell bubble, mimicking a magmatic foam. Blower et al. (2001) highlighted the importance of the concentration-dependence of viscosity and diffusivity during volcanic degassing.

Several experimental contributions on both natural and analogue materials have dealt with bubble-bearing melts. Mourtada-Bonnefoi and Laporte (2004) investigated the effect of decompression rate on bubble number density, by using a crystal and bubble-free volatile-bearing rhyolitic melt. Bai et al. (2008) investigated the evolution of bubbles within a synthetic volatile-bearing basaltic glass, as a function of temperature at ambient pressure.

* Corresponding author. Tel.: +49 (0) 89 2180 4218; fax: +49 (0) 89 2180 4176.
E-mail address: laura.spina@min.uni-muenchen.de (L. Spina).

http://dx.doi.org/10.1016/j.epsl.2015.10.029

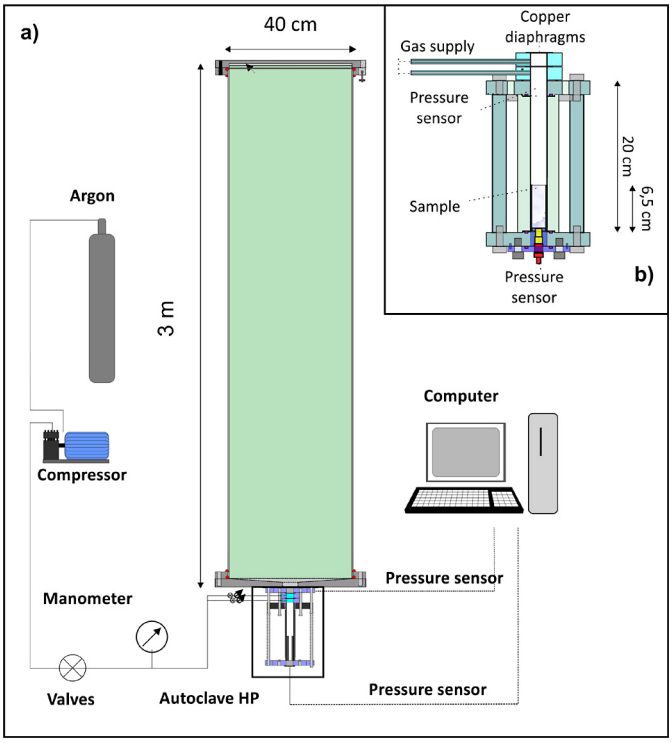

Fig. 1. a) Sketch of the experimental apparatus. The transparent Plexiglas autoclave is fixed below the low pressure tank. Argon gas is supplied through a capillary system, controlled by dedicated valves and manometers. Pressure sensors are located at the top and at the bottom of the autoclave. The black rectangle marks the area shown in b). b) Details of the high-pressure autoclave. (For interpretation of the references to color in this figure legend, the reader is referred to the web version of this article.)

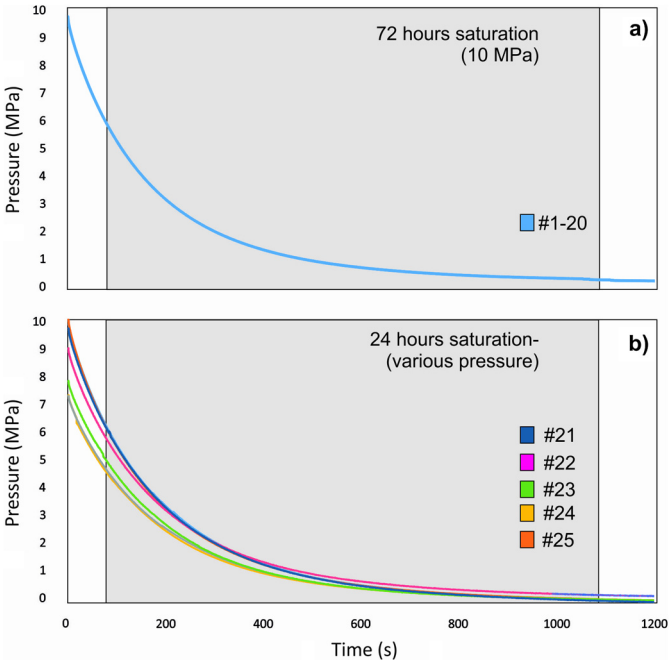

Fig. 2. a) Decompression curves of all the experiments performed with a saturation time of 72 h and saturation pressure of 10 MPa. b) Decompression curves of all the experiments performed with a saturation time of 24 h, and with different saturation pressures. The grey area in a) and b) represent the maximum length of video recording.

Experiments conducted using analogue materials are advantageous, permitting the manipulation of the physical properties of the fluid and the initial thermodynamic state of the system, greatly simplifying investigation of the dynamics of bubbly fluids. As such, rapid decompression experiments on analogue materials have already been used to investigate fragmentation processes (e.g. Ichihara et al., 2002). Experiments have also been performed where the bubble population present prior to decompression was well-known (e.g. Namiki and Manga, 2006, 2008) or where nucleation was induced by decompression (e.g. Lane et al., 2001; Rivalta et al., 2013). Despite progress to date, further investigations are required to map systematically the relative influences of material parameters such as liquid viscosity, amount of dissolved volatiles and suspended solid phases over the pressure and temperature conditions relevant to ascending magmas.

To date studies have focused on rapid decompression conditions in highly viscous systems (e.g. Hurwitz and Navon, 1994; Mourtada-Bonnefoi and Laporte, 2004) rather than low decompression rates in low viscosity systems (e.g. Namiki and Manga, 2006; Rivalta et al., 2013). Yet in natural systems, decompression rates can be as low as <0.02 MPa/s depending on the eruptive style (Fiege et al., 2014 and references within). We therefore present a systematic study of the degassing dynamics of low viscosity analogue magmas during slow decompression conditions, assessing the effect of the varying physical properties on the degassing response of the fluid as a function of viscosity, solid fraction, and particle shapes.

2. Experimental setup, materials and experiments

For investigation of the degassing dynamics of decompression-induced vesiculation in slow ascending magmas, a shock-tube apparatus was employed (Fig. 1), consisting of a high-pressure transparent Plexiglas autoclave connected to a large-volume chamber at ambient pressure. The autoclave is sealed by two diaphragms. The sample (vol. ca. 20 cm^3) is inserted from the bottom of the autoclave (vol. 77.5 cm^3, radius $r = 1$ cm). The system is pressurized under Argon gas (10 MPa) for 24 or 72 h to allow gas diffusion into the liquid. The diffusive equilibration process is monitored via the decay of pressure within the system through a set of manometers. For experiments performed after 72 h, we assume full saturation to be achieved (constant pressure). The equilibrium volatile contents were then estimated (Van der Waals's equation) to be ≈0.0095 mol, corresponding to 1.8 wt%, within the range of water content estimated from melt inclusions in arc and back- arc basin basalts, equal to 0.2–6 wt% (Metrich and Wallace, 2008). The decompression, achieved via a valve system, is characterized by an exponential decay, approximated by two linear segments of the decompression curve: an initial decompression rate of ≈0.02 MPa/s (0–350 s) followed by a slower decompression of ≈0.0009 MPa/s (350 s to the end) (Fig. 2). The pressure in the system is measured by two static pressure transducers. A camera (frame rate = 25 fps) tracks the dynamics of the fluid. The lighting system produces a slight increase in pressure ($<1 \times 10^5$ Pa) and temperature (<0.2 °C/min), for a maximal change of 3.6 °C during decompression.

As a melt analogue, we used a range of Newtonian silicone oils with different viscosities (1, 10, 100 and 1000 Pa s) and a density of 0.97 g/cm^3 (all properties at 25 °C).

To study the effect of crystals on magma degassing, experiments were performed with varying quantities of ceramic microspheres (avg. diameter 83 μm; density = 0.794 g/cm^3). The effect of particle shape was investigated using glass fibres (length = 149 μm; diameter = 14 μm; density = 2.55 g/cm^3). The average aspect ratios of spherical and elongated particles were 1.09 and 10, respectively (Supplementary Table 1). The preparation of homogeneous particle-bearing samples was performed after Cimarelli et al. (2011).

Table 1
Description of the performed decompression experiments.

Experiment number	Viscosity (Pa s)	Particle content (% vol)	Particle type	Saturation time (h)	Saturation Pressure/Initial pressure (MPa)
1	1	0	none	72	10
2	10	0	none	72	10
3	100	0	none	72	9.5
4	100	0	none	72	10
5	1000	0	none	72	10
6	1000	0	none	72	10
7	100	1	spherical	72	10
8	100	1	spherical	72	10
9	100	10	spherical	72	10
10	100	20	spherical	72	10
11	100	30	spherical	72	10
12	100	40	spherical	72	10
13	10	5	spherical	72	10
14	100	0.3	prolated	72	10
15	100	3	prolated	72	10
16	100	7	prolated	72	10
17	100	10	prolated	72	10
18	100	16	prolated	72	10
19	100	20	prolated	72	10
20	100	30	prolated	72	10
21	100	0	none	24	10
22	100	0	none	24	9
23	100	0	none	24	8
24	100	0	none	24	7
25	100	0	none	24	7/10

Four series of experiments were performed to investigate the roles of the 1) liquid viscosity, 2) suspended particle volume fraction, 3) particle shape and 4) amount of dissolved gas on the decompression behaviour of the samples. We initially investigated particle-free samples with different viscosities (1, 10, 100, 1000 Pa s) under constant argon gas pressure (10 MPa) and time (72 h) at sample saturation. Saturation pressure and time remained unchanged in the third and second series. Secondly, we investigated the effect of spherical crystals by loading silicone oil with a viscosity of 100 Pa s with ceramic microspheres at particle volume fraction ϕ, defined as the ratio of particle volume to the volume of particles plus fluid, of 0.01, 0.1, 0.2, 0.3, and 0.4. In the third series we tested the role of particle shape by adding elongated glass fibres (ϕ equal to 0.003, 0.03, 0.07, 0.1, 0.2 and 0.3) to the silicone oil (100 Pa s viscosity). Finally, in the fourth series we investigated the effects of saturation time and pressure through a sequence of experiments with a 24 h saturation time and variable saturation pressure, on 100 Pa s silicone oil (Table 1).

Particle addition influences viscosity (e.g. Mueller et al., 2010). Thus, we measured the viscosity of the suspensions by using a rheometer equipped with a concentric-cylinder narrow-gap geometry (MCR502 from Anton Paar). Measurements were performed at strain rates of 1, 5 and 10 s^{-1} and at temperatures of 21, 25 and 30 °C, in order to fully characterize the rheology of the mixtures over the range of experimental temperature (Fig. 3, Supplementary Table 2). Additional strain rates (0.01 and 0.001 s^{-1}), were used for samples with high solid content ($\phi = 0.40$ and $\phi = 0.33$ for spherical and elongated particles, respectively), to avoid transient effects and slippage along the cylinder walls (see Section 2.1).

2.1. Viscosity measurements

The results of viscosity measurements showed that mixtures with elongated particles have higher viscosities than those with suspended spheres at the same solid content (Fig. 3, Supplementary Table 2), consistent with previous studies (e.g. Mueller et al., 2010).

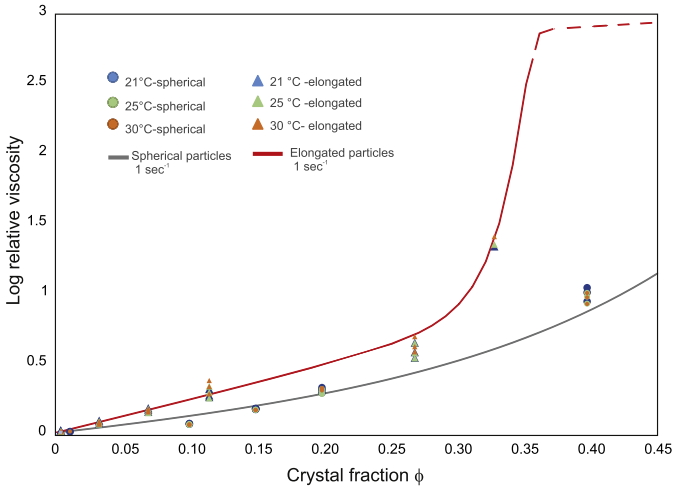

Fig. 3. Characterization of the rheological behaviour of the particle-bearing samples, showing the logarithm of the ratio between the viscosity of solid-bearing mixtures and of the pure liquid versus solid fraction. Blue, green and orange triangles and dots represent the elongated and spherical particle-bearing measurements, respectively, performed at temperatures of 21, 25 and 30 °C. The red and grey lines respectively represent the best fit obtained for elongated and spherical particle-bearing samples by applying the equation of Costa et al. (2009), using strain rates of 1 s^{-1}. (For interpretation of the references to color in this figure legend, the reader is referred to the web version of this article.)

The maximum random packing (ϕ_m) was experimentally determined to be 0.7 and 0.33 for spherical and elongated particles, respectively, lying between the values of $\phi_m = 0.74$ for monodisperse ordered particles and $\phi_m = 0.64$ for a random close packing of spherical particles, and close to the values previously reported for sheared suspension $\phi_m = 0.64$, 0.68 (Mueller et al., 2010 and references therein). The maximum packing fraction measured for elongated particles agrees with the results of Cimarelli et al. (2011). According to Mader et al. (2013), values of 0.41 and 0.65 are predicted for a mono-disperse population of particles with aspect ratios of 10 and 1.09, respectively. While the maximum packing value is only slightly higher than expected for spherical particles, the discrepancy for elongated particles might be due to sample inhomogeneity, i.e. polydisperse size of particles and aspect ratio, as well as to reproducibility limits in sample preparation (Mueller et al., 2010).

In order to parametrize the relative viscosity $\eta_r(\phi)$ of our mixtures, we used the semi-empirical relation valid for concentrated suspensions proposed by Costa et al. (2009):

$$\eta_r(\phi) = \left[1 + \left(\phi/\phi^*\right)^{\delta}\right] / \left[1 - F\left(\phi/\phi^*, \xi, \gamma\right)\right]^{B\phi^*} \quad (1)$$

where ϕ^* is the critical solid fraction at which the effect of crystals becomes dominant and the viscosity values are much higher, γ represents an estimate of the rapidity of the increase in the relative viscosity approaching the value of ϕ^*, B is the Einstein coefficient (i.e. intrinsic viscosity) with a nominal value of 2.5, and δ controls the increase of η_r at $\phi > \phi^*$, and is set at $\delta = 13 - \gamma$ (Costa et al., 2009). F is determined according to the following equation (Costa et al., 2009):

$$F = (1 - \xi) erf\left[\sqrt{\pi}/2(1 - \xi) \cdot \phi/\phi^* \cdot \left(1 + \phi^{\gamma}/\phi^{*\gamma}\right)\right] \quad (2)$$

The best-fit parameters ϕ^*, γ, ξ computed for equations (1) at strain rates of 1 s^{-1}, are equal to 0.65, 2, 1×10^{-3} for spherical particles-bearing mixtures, and 0.34, 12, 1×10^{-3} for elongated particles-bearing mixtures, respectively.

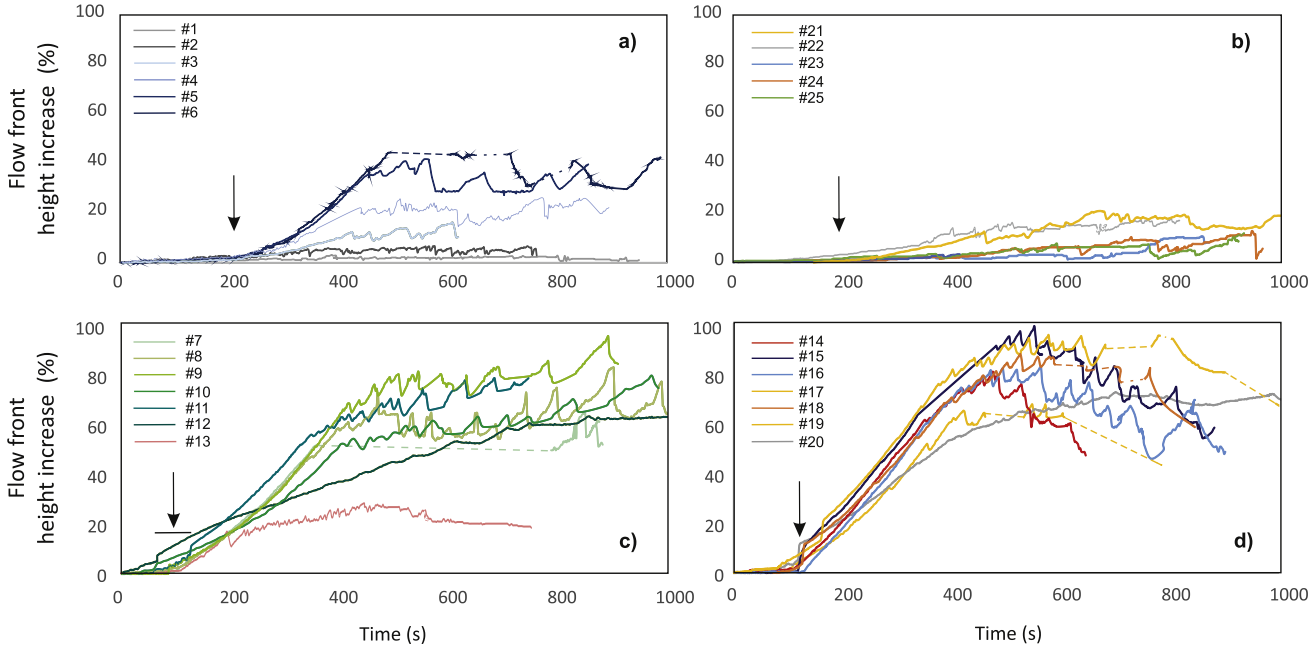

Fig. 4. Flow front height percentage increase measured for a) pure silicone oils with different viscosities; b) pure silicone oils with viscosity equal to 100 Pa s, saturated for 24 h at different pressure; c) spherical particle-bearing mixtures; d) elongated particle-bearing mixtures. The legend in each graph reports the experiment number according to Table 1. The black arrows mark the beginning of foam build-up phase. Data were collected with a sampling rate of 0.5 Hz. At each time-step the error related to the picking of the fluid front height level lies within the point. Note that time zero corresponds to the beginning of the camera recordings, when reaching a pressure of 6 MPa (roughly 70 s after opening the valve).

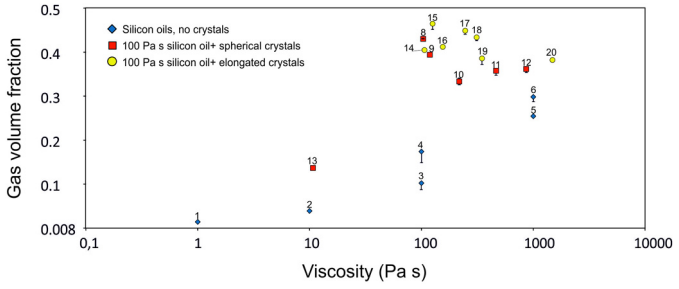

Fig. 5. Plot of the gas volume ratio of pure silicone oils (blue diamonds) and spherical (red square) and elongated (yellow dots) particle-bearing samples. The experiment number is reported above the data point. The error bars indicate the maximum error on the volume computation due to the convex shape of the rising fluid column. When error bars are missing, error is smaller than the symbol. (For interpretation of the references to color in this figure legend, the reader is referred to the web version of this article.)

3. Experimental results

3.1. General remarks

The dynamics of bubbly fluid were investigated through image analysis. In all experiments, delayed nucleation occurred, therefore video recordings were started when the system reached a pressure of 6 MPa, tens of seconds after decompression initiation. Bubbles nucleate and grow ("nucleation phase", Section 3.2), until they develop a foam layer at the top. Bubble expansion in the foam accelerates the vertical ascent of the fluid ("foam build-up phase", Section 3.3). Eventually, when coalescence becomes dominant, the foam stops ascending, and oscillates around an equilibrium level (Section 3.4). Here, we focus mainly on the fluid dynamics during nucleation and foam build-up. A detailed description of the scaling of the dynamic processes within our experiments to the volcanic system is provided in Section 4.3.

In order to analyse quantitatively the dynamics of the ascending fluid, we parameterised the percentage increase in the flow front height of the column using the following equation:

$$\Delta L_t = \left[\left(Lf(t) - L_0\right)/L_0\right] \cdot 100 \quad (3)$$

where L_0 represents the initial length of the sample, and $Lf(t)$ the length of the sample at a given time t. The percentage increase ΔL_t has been estimated, with a sampling rate of 0.5 Hz for a central point along the fluid surface. Fig. 4 shows plots of ΔL_t versus time for each experiment reported in Table 1. The height of the fluid surface has been used previously to parametrize the behaviour of bubbly fluid (e.g., Namiki and Manga, 2008; Su, 2005 and references therein).

The expansion of the sample is almost entirely due to the exsolution and expansion of the gas phase. Assuming a flat liquid surface, we determined the percentage of volume increase (Fig. 5) at a given time by multiplying ΔL by a constant factor πr^2. However, the flow front typically displays a parabolic profile. The maximum error related to this assumption was evaluated by comparing the values of volume fractions obtained by taking two lateral points (each 5 mm apart) as a reference; the related error is minor (Fig. 5).

3.2. Nucleation phase

The degassing history of decompressed analogues begins with the delayed appearance of isolated bubbles in the uppermost section of the sample ("first nucleation"). The ability to identify a nucleated radius depends on camera resolution. We term "nucleation" as the first appearance of a bubble with the smallest visible radius (0.05 mm). Fig. 6 shows the pressure at which the first nucleation event was observed for experiments saturated for 24 h (a) and 72 h (b). The pressure of nucleation varies with saturation time and pressure. The ΔP required for the 24 and 72 h experiments is in the range 3–5 MPa and 4.4 to 6 MPa, respectively.

Once nucleated, bubbles start to grow and ascend toward the surface. Bubble growth rates were measured in pure silicone oils,

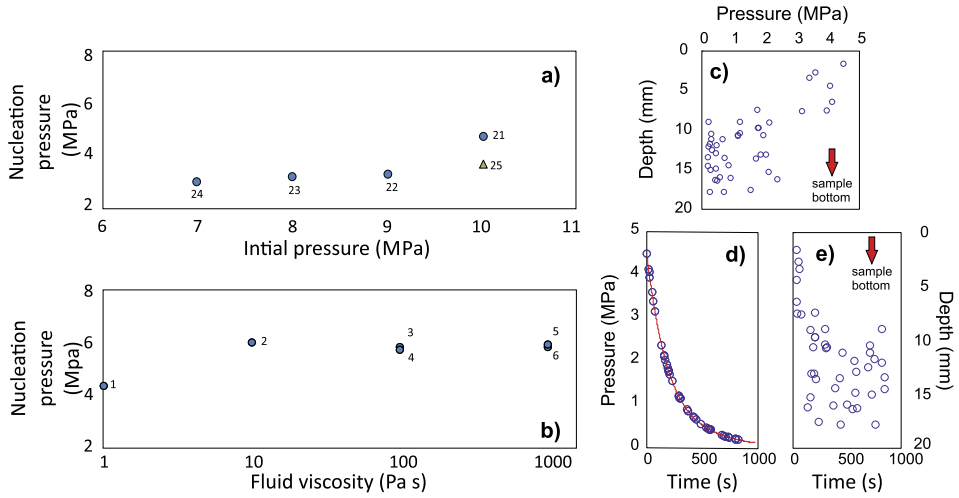

Fig. 6. a) Nucleation pressure of experiment 21 to 25 versus initial decompression pressure. b) Nucleation pressure of experiment 1 to 6 versus viscosity. c)–e) Plot of pressure, time and depth for several nucleation events occurring during experiment 21 (24 h saturation). Zero depth is coincident with the initial surface of the liquid column. The time zero corresponds to the beginning of the camera recordings, when reaching a pressure of 6 MPa (roughly 70 s after opening of the valve). The migration of the nucleation surface toward deeper levels is visible from plate e).

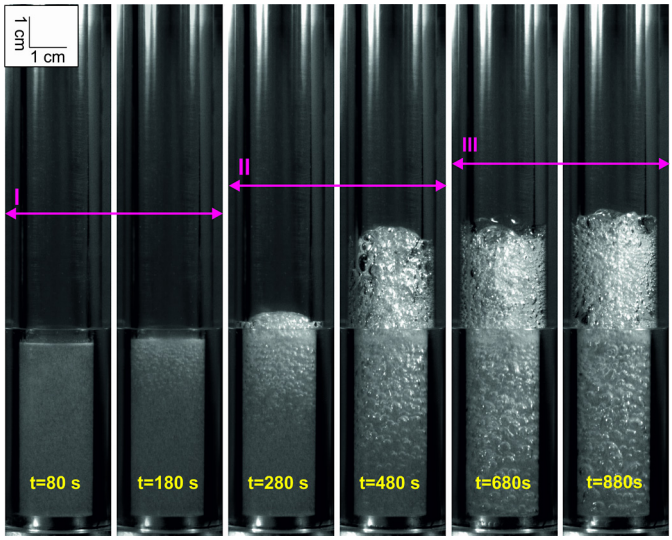

Fig. 7. Snapshot picturing the foam ascent phase from experiment 8. Pink arrows and roman numbers indicate the phase of the bubbly fluid at the time shown in the picture (I: nucleation, II: foam build-up, III: foam oscillation). (For interpretation of the references to color in this figure legend, the reader is referred to the web version of this article.)

on at least 10 bubbles picked at times between their initial appearance until bubble–bubble contact or until reaching the surface of the fluid. Growth rates increase throughout the decompression, from values of 10^{-3} mm/s up to 10^{-1} mm/s for later nucleated bubbles (Supplementary Fig. 1). Bubble ascent rates range from less than 10^{-2} mm/s for higher viscosity silicone oils (experiments 4 to 6) up to $10^{-1} - 1$ mm/s for lower viscosities (experiments 2 and 1, respectively).

Throughout the decompression, multiple nucleation episodes occur. Some bubbles nucleate between previously generated nuclei. A migration of the exsolution level downwards is evident in all the experiments (an example in Fig. 6e).

Due to the intrinsic opacity of the mixtures, we did not quantify nucleation pressures for particle-bearing experiments. Nevertheless, we observed that the presence of crystals enhances the early formation of a larger number of small spherical bubbles (Fig. 7). In experiments performed within the dilute regime (experiments 7, 8 and 14), where mixtures are still partially optically transparent, bubbles became visible at ~6 MPa, and a progression of the nucleation surface toward the bottom of the sample was visible.

3.3. Foam build-up phase

After a certain quantity of bubbles have nucleated, an abrupt change in the rise speed of the mixture is observed, as a foam is produced at the top of the sample. This is reflected by a kink in the plot of flow front height against time (black arrows in Fig. 4). We infer that this time marks the beginning of the foam build-up phase. For experiments 1 and 2 no foam formed and thus no foam build-up was observed. In this case, the flow regime is characterized by an almost radially uniform profile of the fluid surface and uniform bubble-size distribution.

For particle-free experiments (runs 3 to 6), we collected images corresponding to the time when the kink in ΔL was observed (i.e. at the beginning of foam build-up phase). Then we analysed sample vesicularity ϕ_b at that stage by measuring the surface area of bubbles lying in the focal plane, against the area of the section of the sample affected by nucleation. Vesicularity ranged from ϕ_b of 0.19 and 0.27 for experiments 3 and 4, and from 0.23 to 0.21 for experiments 5 and 6. Even though we could not measure it, we expect the vesicularity to increase significantly, when a foam is fully developed. Foam gas volume fractions of 0.74 to >0.90 have been reported, depending on bubble shape and polydispersity (e.g. Bhakta and Ruckenstein, 1997).

The starting time and the maximum volume fraction of the foam build-up depends on the liquid properties (mainly liquid viscosity), particle content and shape (i.e., mixture rheology). An example is shown in Fig. 5, where particle content is plotted against gas volume ratio, computed at the end of the foam build-up phase, for particle-free and particle-bearing experiments (72 h saturation). For experiments 12 and 20, this point corresponds to the beginning of the flat section of the curves. For experiments 1 and 2, we take as a reference the gas volume fraction immediately after the initial liquid expansion due to nucleation. In either case, gas volume ratio does not change remarkably during the experiments.

In pure silicone oil experiments (Fig. 4a), viscosity controls the ascent velocity and the total bubble volume fraction. The addition of small quantities of particles (e.g. experiments 7, 8 and 14 in Fig. 4c, d) dramatically increases bubble volume fraction at the end of the second phase (Fig. 5). Nonetheless, there is no linear relationship between the increase in both particle content and gas

volume fraction, suggesting that the change in rheology might play a dominant role for high solid-volume fractions (see Section 4.2).

Additionally, the observation that experimental gas volume fractions are systematically lower than perfect gas law expansion reflects the importance of the nucleation kinetics. A volume of gas of 2.72×10^{-5} m^3 is expected for 0.0095 moles of argon at 25 °C/0.8 MPa (the temperature/pressure conditions at ≈470 s, when foam build-up mainly approaches its end). Considering the initial liquid fraction, this is equivalent to a gas volume fraction of 57%, slightly higher than the maximum values in Fig. 5 and strikingly higher than for pure liquid experiments. Individual differences in the deviation of experimental points of Fig. 5 from theoretical values reflect the effect of different physical properties on the nucleation kinetics.

3.4. Foam oscillation phase

The foam ascent is interrupted when bubbles collapse to form a "slug-type" pocket of gas, either at the base or within the foam, enabling permeable outgassing (Fig. 8). Consequently, a drop in the fluid level is observed, until newly nucleated bubbles reach the foam, restoring its thickness, subsequently inducing another bubble collapse, causing periodical oscillations of the fluid level. The time scale of such oscillations reflects the time scale of bubble coalescence and is dependent on the mixture properties (Fig. 4).

4. Discussion

4.1. Bubble nucleation and growth

Bubble nucleation was observed in all experiments. Supersaturation conditions and the resultant generation of first bubbles, was generally reached tens of seconds after the decompression started. As gas solubility in our silicon oil is independent of viscosity, the main variables affecting nucleation are saturation time and pressure. Fig. 6a illustrates a slight tendency of the nucleation pressure to increase with saturation pressure. Decreasing saturation time produces a decrease in the nucleation pressure (Fig. 6a, b).

Bubble nucleation occurs initially at the top of the sample, and successively nucleation deepens (i.e. Fig. 6e). A similar pattern, attributed to interfacial degassing, was previously observed in decompression experiments using Gum Rosin-Acetone (hereafter GRA) mixtures (Phillips et al., 1995). Nucleation is facilitated in proximity to the free surface, and a vertical gas profile develops in its wake. The foaming at the top of the sample steepens the concentration gradient, and this in turn enhances bubble nucleation in the region immediately below the foaming. Although a direct comparison with our experiments is not possible, numerical models imply that a deepening of the exsolution level is likely in volcanic systems. Folch (2000) performed numerical simulations of an isolated rhyolitic magma chamber connected with a central conduit, and obtained a deepening of the exsolution level in response to an exponential decrease of the pressure at the conduit entrance. More recently, Girona et al. (2014) have suggested that quiescent steady-state degassing might induce a gradual deepening of the exsolution level, reducing by several MPa the pressure at the reservoir in a timeframe of months to years.

The addition of particles, both spherical and elongated, to silicone oil strongly enhances heterogeneous bubble nucleation (Hurwitz and Navon, 1994). Comparison of images taken at equivalent times for particle-free and particle-bearing experiments reveals a larger number of smaller bubbles in the latter (Fig. 7, Supplementary Fig. 2), consistent with the expected effect of particles in enhancing heterogeneous nucleation. This is already evident at small particle percentage (experiments 7, 8 and 14). Clearly, the effect of particles in the system cannot be neglected in any realistic model.

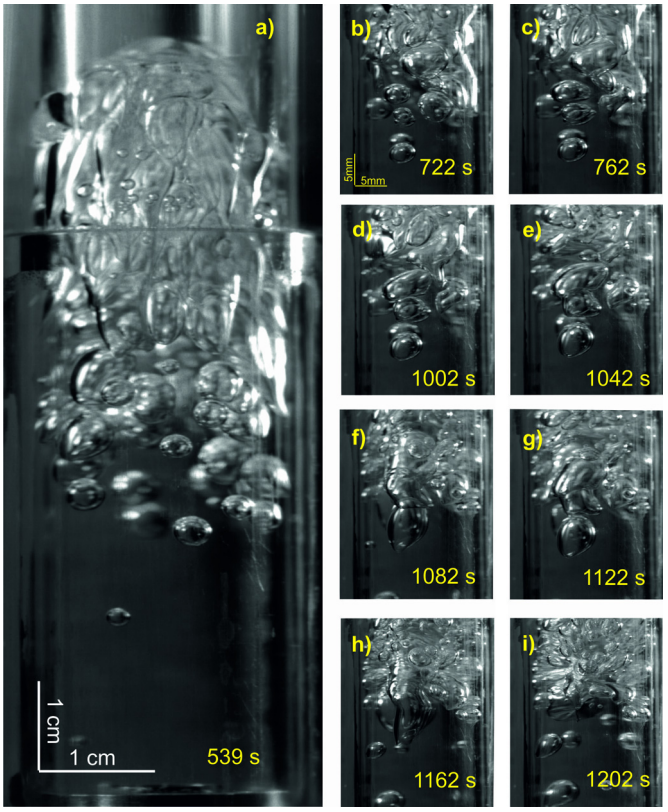

Fig. 8. a)–e) Snapshots from experiment 6. b)–i) Sequence of snapshots showing the interaction of equal-sized bubbles at the base of the foam layer to form a "slug-type" bubble. The slug generally ascends faster within the foam and burst at the surface, or below it, causing the foam to collapse.

No explosive fragmentation was observed in any of our slow decompression experiment. In contrast, Rivalta et al. (2013) reported occasional observations of delayed nucleation and explosive expansion for slow decompression experiments (as low as 50–400 Pa s^{-1}) in 30, 35 and 40 wt% GRA mixtures. They attributed this evidence to the large supersaturation conditions caused by homogeneous or inefficient heterogeneous nucleation. We argue that the discrepancy with our results derives from the significantly lower volatile content (≈1.8 wt%) and slightly higher diffusivity (1.4×10^{-6} cm^2/s) characterizing our experiments. It is noteworthy that this diffusivity value is within the range for gases in silicate melts at the relevant temperature (10^{-5}–10^{-9} cm^2/s; e.g. Sparks, 1978).

4.2. Foam build-up and effects of varying state properties

Once a sufficient number of bubbles have grown, the mixture abruptly accelerates due to bubble volume expansion at ever faster rates as evident in the flow front height profile (Fig. 4). For particle-free experiments, the vesicularity at initial foam build-up ranges between 0.19 and 0.27. Bai et al. (2008) performed degassing experiments by heating basaltic samples at atmospheric pressure and found that for $\phi_b > 0.18$ bubble coalescence and expansion occur simultaneously; this phase lasts for about 100–200 s, during which bubbles create a foam. In our experiments, the increase in the expansion velocity of the mixture, (initiation of foam build-up), is related to bubble proximity. Vesicularity increases to a threshold (here, $\phi_b = 0.19$–0.27), above which bubbles are influenced by the surrounding bubble swarm, and expand faster, due to the diminished confining pressure. Proussevitch et al. (1993) found that enhanced growth rate results from thinner shells of viscous melt, as a smaller dynamic resis-

tance is offered to bubble growth. Similarly, Barclay et al. (1995) demonstrated that the expansion time of an isolated bubble (lower vesicularity) is much higher than that of a bubble surrounded by a thin shell of magma (higher vesicularity). Vesicularity measured in the solidifying Alea lava lake (Hawaii) was found to be as low as 40% near the surface and 11% below 3 m (Peck, 1978), suggesting that such low vesicularities may indeed also characterize magmas at very shallow levels.

In pure silicone oil experiments (3 to 6) the beginning of the foam build-up is evident at 200–225 s in Fig. 4a where the gas volume fraction increases with mixture viscosity. This may be related to the combined effect of slower bubble rise and slower liquid drainage out of the bubble walls, increasing the timescale for gas movement (Belien et al., 2010). The time required for the fluid interstitial between two bubbles to drain, leading to wall collapse and coalescence, is longer for higher fluid viscosities (Nguyen et al., 2013). The expansion of such trapped gas bubbles, allows for the development of a larger foam layer at the top of the fluid column, whose growth causes the observed rapid ascent of the mixture.

The three-phase mixtures, i.e. silicone oil + crystals + bubbles, exhibit further complexities. The addition of particles did not decrease gas permeability of the sample as evidenced by the lack of any delays in nucleation and foam build-up, as well as being implied by the similarity of the pressure decay curves during saturation of samples with and without particles. On the contrary, the enhancement of nucleation due to the solid particles within the fluid causes earlier foam build-up (60 to 130 s; Fig. 4c and d) for both spherical and elongated particles.

The behaviour of three-phase mixtures has been extensively studied in "bubble column reactors" (cylindrical vessels with a gas distributor at the base), where the bubbles are delivered into either a liquid phase or a liquid–solid suspension (Kantarci et al., 2005). A decrease of the so-called gas "hold-up" (i.e. gas volume fraction) is observed with increasing concentration of solids (e.g. Mena et al., 2005). In fact, particle loading might play a dual role on the gas phase, as with increasing solid content, the gas hold up was first found to increase, and then subsequently to decrease, with local maxima at ϕ equal 0.20–0.30 (Mena et al., 2005) and less than 0.10 (Bukur et al., 1990), respectively. Banisi et al. (1995) have suggested that small amounts of fine particles, as well as large numbers of large particles, increase gas volume fraction due to the suppression of coalescence from the fine particle matrix, or in the latter case, due to the breakup of large bubbles by particles.

At low particle contents, the crystal liquid mixture can be treated as a fluid with higher effective density and viscosity than the liquid phase (Belien et al., 2010), but for higher crystal fractions, several additional effects might play a role. Solid particles reduce the space available for bubble expansion, generating critical conditions at lower values of vesicularity. For bubble diameters d_b much larger than the dimension of the particles d, and particularly when $d_b > d/\phi^{1/3}$ (Mena et al., 2005), as in the present study, the change in the average density of the mixture might affect the buoyancy of particles. Reduced bubble speed and therefore an increase of coalescence have been suggested to be caused both by the change of effective viscosity of the solid–liquid suspension, and by bubble–particle collision (Mena et al., 2005).

In all of our particle-bearing experiments, gas volume fraction is higher than in particle-free experiments (Fig. 5). This stands in apparent contrast with the literature but can be explained by the fact that particles allow for enhanced nucleation of a larger number of small bubbles, thereby increasing the gas volume fraction. Additionally, a distribution of smaller and more pervasively distributed bubbles leads to a decrease in bubble packing efficiency. Smaller bubbles are characterized by a greater Laplace pressure than larger ones, thus they are less deformable (Nguyen et al., 2013), and this effect contributes to the increase in gas volume fraction as well.

Okumura et al. (2012) found that outgassing was not effective in corundum-bearing rhyolite with <70% vesicles, due to the low corundum contact angle inhibiting heterogeneous nucleation. In contrast, our particle-bearing experiments provide ample evidence of heterogeneous nucleation.

Similarly to Mena et al. (2005), we initially observe an increase in the total gas volume fraction with solid loading for spherical particles (experiments 8 and 9), and successively, its relative decrease, for ϕ value equal or greater than 0.20. Elongated-particle-bearing experiments behave similarly, even though they display a much more complex gas volume fraction pattern (Fig. 5), likely related to settling of the much denser elongated particles during the experiments (see Section 2). The observed decrease of gas volume fraction with solid content is consistent with literature data (e.g. Su, 2005). Based on the relative proportion and densities of the components (e.g. Ruzicka, 2006), for spherical particle-bearing mixtures a density decrease of only 2–7% is expected for $\phi = 0.01 - 0.4$. On the contrary, the density of elongated particle-bearing mixtures increases up to 49% for $\phi = 0.33$, increasing bubble buoyancy. For both particle shapes, at high particle loading, bubble expansion is prevented by the volume of the solid network in the liquid, leading to a much higher bubble concentration rather than for low particle loading, and to bubble coalescence and breakup. Accordingly, measurements performed in high crystallinity (>40%) lapilli-sized scoria from ordinary (non-paroxistic) activity at Stromboli, have revealed the existence of irregular, tortuous, channel-like large bubbles, adapting to the porphyritic crystal framework. Such vesicles result from extensive coalescence of small, interconnected bubbles at the percolation threshold (Polacci et al., 2008).

Remarkably, at the highest solid contents of both spherical and elongated-particle-bearing mixtures of our dataset (e.g. experiments 12 and 20) the gas volume fractions are low, and the curves in Fig. 4c, d exhibit low ascending velocities of the fluid. This might be related to the muffling effect on the gas phase of the solid fraction. Similar curves were observed for the vertical expansion of GRA by Stix and Phillips (2012), particularly for 15 wt% GRA (high viscosity sample). We too observe a motion of the fluid front resembling "stick-slip" behaviour, with alternately high and low velocity of the expanding fluid. Consistent with the above, this behaviour was observed in our experiments only for high viscosity mixtures.

Finally, all the curves in Fig. 4d (except experiment 20), show a decay after a maximum value of fluid column increase is reached. According to Tang and Heindel (2005), the additional mechanisms through which fibres influence bubbles are: i) by increasing bubble residence time through the development of a fibre network; ii) by favouring gas channelling (for high mass fraction) and iii) in suppressing bubble breakup by damping turbulence in the fluid. Additionally, for an initial random distribution of particles, the re-orientation of the elongated particles with the flow direction might also affect the degassing properties of the fluid. In fact, elongated particles rotate about the vorticity vector of the flow (Jeffery, 1922). In a Newtonian fluid, the fibres rotate about their axis of symmetry exhibiting as they do precession around the vorticity axis (Astruc et al., 2003). Natural examples of elongated crystals aligned with the flow direction in granite batholiths and lava flows have been documented in previous studies (e.g. Ventura et al., 1996). The preferential alignment of particles with the upward direction of the flow, achieved through time, might be an explanation for a more effective gas escape in our elongated particle-bearing experiments.

Alternatively, "flocculation", defined as the unevenness of a fibre network, as well as the process of growth of the fibre network

Table 2
Comparison between laboratory and volcano-scale dynamic conditions. The non-dimensional numbers were computed for pure silicone oils from the start of the decompression until the development of the foam (phase I). The corresponding values at the volcano-scale condition are given for basaltic-intermediate composition and for the initial flow expansion below the fragmentation level.

Non-dimensional number	Experimental value	Volcano-scale condition
$Re = D\rho U/\eta$	10^{-7}–10^{-5}	$< 10^3$
$Re_b = \rho D_b U_b/\eta$	10^{-10}–10^{-3}	$<<1$
$E_0 = g\Delta\rho D_b^2/\sigma$	10^{-3}–10^{1}	$10^{-3} < 10^6$
$M_0 = g\eta^4\Delta\rho/\rho^2\sigma^3$	10^{2}–10^{14}	10^{2}–10^{15}
$C_a = \eta u_e/\sigma$	10^{-5}–10^{-1}	Ca$<<1$

Non-dimensional numbers: Re = Reynold number, Re_b = Reynold bubble number, E_0 = Eötvos bubble number, M_0 = Morton bubble number, Ca = Capillary number.
Parameters list: D = Conduit diameter, U = fluid velocity, η = fluid viscosity, ρ = fluid density, U_b = bubble velocity, D_b = bubble diameter, $\Delta\rho$ = absolute value of density difference between bubbles and fluid phase, σ = surface tension, u_e = expansion velocity.

itself (Kerekes et al., 1985), and segregation of fibres into the fluid, leading to preferential paths for gas escape, may develop. The development of regions characterized by different local mass density affects the behaviour of the gas phase. When the fibre mass fraction is high, gas channelling occurs, either by breakup of the network by larger bubbles (non-static channel) or by formation of different gas–escape pathways active on a timescale of seconds to minutes (e.g. Tang and Heindel, 2005), and thereby increasing degassing efficiency.

4.3. Implications for volcanic eruptions

The analysis of our suite of experiments enables the constraining of the contribution of different physical properties, i.e. fluid viscosity, particle content and shape, and saturation state, to the behaviour of the gas phase above the gas exsolution level.

Upon decompression, the dynamics of volatiles in our analogue system featured the sequence of bubble nucleation, bubble growth, and finally the development of a foam expanding within the conduit. Similarly, the generation of an expanding foam flow is expected for magmas, at pressure lower than the exsolution pressure of water and other gas phases (e.g. Massol and Jaupart, 1999; Lane et al., 2001). To evaluate the applicability of our results to fluid dynamics within the shallow volcanic conduit, we need to consider the balance of forces acting on each fluid volume.

Table 2 compares our experimental system (crystal-free experiments) to mafic magma using the ratio of the forces acting 1) on the fluid and 2) on single bubbles, from the initiation of decompression to foam generation. Calculated Reynolds numbers for phase I are $\ll$1, coherent with the observation that, in volcanic systems, the initial flow expansion below the fragmentation level is laminar (Massol and Jaupart, 1999). The relative ratios of inertial, viscous, surface tension, buoyancy and capillary forces have been evaluated through Reynold, Eötvos, Morton bubble numbers and Capillary number for a range of bubbles diameters (Table 2), and compared to natural estimates (Manga and Stone, 1994; Belien et al., 2010; Del Bello et al., 2012; Moitra et al., 2013; Nguyen et al., 2013). The experimental non-dimensional numbers in Table 2 were computed neglecting the role of bubbles in the rheology of the fluid. Indeed, given the moderate bubble concentration ($\phi_b \ll 0.45$) and the associated low capillary numbers (Ca$\ll 0.3$) during phase I, the increase in viscosity due to the presence of bubbles is weak (<25%; Manga et al., 1998) to negligible (Lane et al., 2001). During phases II and III, a more developed foam-flow is established. Massol and Jaupart (1999) noted that short-scale longitudinal and radial variations are expected within the foam, precluding us from extending the nondimensional analysis to these phases. Furthermore, for non-dilute suspensions the bubble interactions affect bubble shape and therefore the suspension rheology cannot be easily predicted (Llewellin and Manga, 2005 and references therein). Nonetheless, we adopt an approach similar to Lane et al. (2001) and, given that properties of the bubbly fluid both in nature and in our experiments are evolving in the same direction during degassing, we expect the dynamic similarity to be valid during phases II and III.

We recall here that in our experiments, the main driving force of bubble expansion is decompressional growth, as expected for shallow conduit dynamics, where pressures are low, and decompressional expansion dominates over diffusional (Sparks, 1978). At higher depth, or for small bubbles, diffusional growth dominates.

Additionally, we mainly investigated decompression rates on the order of 2×10^4 Pa s^{-1}. According to Namiki and Manga (2006) for decompression rates of the bubbly column equal to 20–200 Pa s^{-1}, 2×10^4 Pa s^{-1} and $>10^6$ Pa s^{-1}, effusive eruptions, explosive eruptions and fragmentation are expected, respectively. Consequently, we expect fragmentation to occur at higher decompression rates.

The effect of particle loading on the gas phase also depends on the relative proportions and geometry. A useful indication of the style of gas–solid interaction is given by the ratio between bubble diameter and particle width: ψ (Belien et al., 2010). Assuming a minimum bubble radius of 0.05 (detection threshold) and a maximum of 5 mm, we obtain a value of ψ ranging between 6.17–61.7 and 10.41–104.1, for elongated and spherical particles-bearing mixtures, respectively. Therefore, for a crystal population of 100 μm – which is the lower threshold for phenocrysts (Murphy et al., 2000), our results are valid for bubbles sized 0.6–6 mm and 1–10 mm, for elongated and spherical particles respectively. Alternatively, assuming as higher threshold a crystal size of 5 cm, i.e. the lower size for megacrysts (Johnson and Glazner, 2010), the experiments mimic the interaction of crystals with bubble sized 6–60 cm and 0.5–5.2 m for elongated and spherical particle-bearing experiments, respectively.

The effect of crystallinity on degassing has important implications for shallow conduit dynamics. At Stromboli volcano, a shallow crystal-rich (ca. 50% crystallinity) magma is thought to reside over a volatile-rich and crystal-poor one (Bertagnini et al., 1999). The crystal mush contributes to trap small bubbles, thereby increasing gas hold-up; experimental data highlighted the critical role played by the high crystal content of the shallow Stromboli magma in regulating gas flux through the system (Belien et al., 2010). Similarly, at Mt. Yasur, interaction between partially crystallized magma (alternatively recycled rocks) and the rapidly ascending magma was inferred to occur at shallow depth (Kremers et al., 2012). Nevertheless, crystals not only influence the movement of ascending bubbles, but also facilitate their nucleation (Hurwitz and Navon, 1994), and both effects were taken into account in our experiments. We demonstrated that gas volume ratio is maximum in diluted and semi-diluted regimes ($\phi < 0.25$ and $\phi < 0.13$, for spherical and elongated particles, respectively) and decreases in the concentrated regime. At very high crystal content ($\phi = 0.40$ and $\phi = 0.30$ for spherical and elongated particles, respectively) the motion of the fluid front is damped and indeed, basaltic lavas with ϕ bigger than 0.55 have rarely been reported (Marsh, 1981). Hence, we stress that crystal content needs careful consideration when modelling gas dynamics within the conduit, where partially crystallized magma is often likely to reside.

Our experiments explicitly take into account the effect of particle loading on degassing in heterogeneous nucleation condition, i.e. the solid phase existed prior the decompression, thus promoting bubble nucleation. Nonetheless, crystallinity may increase in response to the drop in the liquidus temperature due to volatile exsolution. Degassing promotes crystallization, which in turn accelerates bubble nucleation by increasing water concentration in the

melt fraction (Simakin et al., 1999). However, this effect is more evident for silicic melts, as the influence of water on the liquidus temperature of more mafic melts is rather small (Simakin et al., 1999).

By comparing the degassing history of elongated and spherical particles, we inferred a higher efficiency of the former in favouring gas escape, with important implications for magmas bearing elongated crystals. Alignment of phenocrysts or groundmass crystals was abundantly documented (e.g. Smith, 2002), as well as reorientation of pre-existing microlites in simple shear flow (Mangan, 1998). Despite the extensive discussion on the effect of crystals shape on magma rheology (e.g. Mader et al., 2013; Cimarelli et al., 2011), the results on degassing of a network of acicular crystals remain underinvestigated.

Finally, another striking feature of our experiments is the observation of a cyclic foam oscillation, with a periodicity related to the time-scale of bubbles collapse, within the foam, in relatively bigger bubbles, which rise faster than the neighbour swarm of bubbles, and burst at/close to the surface. As evident from Fig. 4, the periodicity is related to the physical properties of the fluid, with important implications for modelling oscillatory phenomena at low viscosity volcanoes. For example, lava lakes are often characterized by cyclic inflation–deflation of the magma free surface, i.e. gas piston activity (Swanson, et al., 1979). According to Dibble (1972), the origin of the gas piston activity is related to the occurrence of a periodical collapse and formation of a foam layer at the top of the lava column. This evidence is in agreement with our experimental observations, and requires further investigation.

5. Summary

We have experimentally investigated the effect of physical properties on the decompressive response of analogue fluids undergoing slow decompression. Here we summarize the main observations.

- The degassing response of the volatile-bearing samples to the decompression was characterized by three phases (nucleation, foam build-up, foam oscillation), corresponding to well-defined stages of the ascent history.
- Delayed nucleation is observed from the opening of the system that is dependent on the saturation condition (higher delay for lower saturation time and pressure).
- Bubble expansion rate increases sharply as they approach each other, leading to a quick fluid ascent (foam build-up). The vesicularity at that stage, estimated for pure silicone oils, lies in the range 0.19–0.27. The timing at which foam build up occurs is quite homogeneous in silicone oil (200–225 s). Both spherical and elongated particle-bearing experiments show anticipated foam build-up (60–130 s), ascribed to the enhanced (heterogeneous) nucleation due to the addition of particles.
- When coalescence phenomena become dominant, the fluid either slows down or stops its ascent and starts oscillating in response to the periodical collapse of the foam into a slug-type bubble, which bursts at the surface or within the foam.
- Particle loading plays a dual role in the degassing dynamics; at low solid fraction, the addition of particles increases the gas volume fraction, accordingly with the increased bubble number density (here only qualitatively assessed). As the solid volume fraction increases, the enhancement in the nucleation due to the particles no longer balances the hindering role played by the increase in viscosity and by the volume occupied by solids.
- Elongated particles showed an increased degassing efficiency compared to the spherical ones. This evidence might be related to the ability of the shear applied from the ascending mixture to orientate the particles, causing a decrease in the viscosity hence favouring gas escape or, alternatively, to gas channelling and flocculation.
- By comparing the four series of experiments, we found that the presence/absence of particles plays the most dramatic role in determining the decompressive response of the mixture, because it strongly controls the total released gas and therefore, the extent of mixture ascent. Similarly, saturation conditions (time and pressure) affect the magnitude of degassing; i.e. poorly saturated samples will have a low level of bubble activity. The total amount of particle loading plays a secondary role at low and medium concentration, where we observed similar degassing history and values of gas volume ratios, but affect strongly the motion of the fluid at high particle concentration. Particles' shape influences the dynamics of degassing only on a long-term scale: provided enough time for rearrangement of the particle network, elongated particles increase the efficiency of degassing.
- Using scaling considerations, we demonstrate that our results are valid for basaltic-intermediate magmas at shallow depth. The importance of particles in modulating the eruptive dynamics has been previously highlighted in volcanic systems (Stromboli: Bertagnini et al., 1999; Mt. Yasur: Kremers et al., 2012). Here we confirm the primary role played by crystallinity in shallow conduit dynamics.

Acknowledgements

We thank A. Namiki and an anonymous reviewer for their careful review of the manuscript, and A. Vona for fruitful discussions. LS and BS have received support of the European Commission (FP7-MC-ITN, grant number 289976: NEMOH). CC acknowledges AXA Research Fund and Marie Curie Grant BEACon (No. 235328). BS and DBD acknowledge funding from the EC FP7 grant agreement No. 282759 (VUELCO). DBD acknowledges the support of an ERC Advanced Investigator Grant (EVOKES – No. 247076).

Appendix A. Supplementary material

Supplementary material related to this article can be found online at http://dx.doi.org/10.1016/j.epsl.2015.10.029.

References

Astruc, M., Vervoort, S., Nouatin, H.O., Coupez, T., Puydt, Y.D., Navard, P., Peuvrel-Disdier, E., 2003. Experimental and numerical study of the rotation and the erosion of fillers suspended in viscoelastic fluids under simple shear flow. Rheol. Acta 42 (5), 421–431.

Bai, L., Baker, D.R., Rivers, M., 2008. Experimental study of bubble growth in Stromboli basalt melts at 1 atm. Earth Planet. Sci. Lett. 267 (3–4), 533–547.

Bhakta, A., Ruckenstein, E., 1997. Decay of standing foams: drainage, coalescence and collapse. Adv. Colloid Interface Sci. 70, 1–124. http://dx.doi.org/10.1016/S0001-8686(97)00031-6.

Banisi, S., Finch, J.A., Laplante, A.R., Weber, M.E., 1995. Effect of solid particles on gas holdup in flotation columns—I. Measurement. Chem. Eng. Sci. 50, 2329–2334.

Barclay, J., Riley, D.S., Sparks, R.S.J., 1995. Analytical models for bubble growth during decompression of high viscosity magmas. Bull. Volcanol. 57, 422–431.

Belien, I.B., Cashman, K.V., Rempel, A.V., 2010. Gas accumulation in particle-rich suspensions and implications for bubble populations in crystal-rich magma. Earth Planet. Sci. Lett. 297 (1–2), 133–140. http://dx.doi.org/10.1016/j.epsl.2010.06.014.

Bertagnini, A., Coltelli, M., Landi, P., Pompilio, M., Rosi, M., 1999. Violent explosions yield new insights into dynamics of Stromboli volcano. Eos Trans. AGU 80 (52), 633–640.

Blower, J.D., Mader, H.M., Wilson, S.D.R., 2001. Coupling of viscous and diffusive controls on bubble growth during explosive volcanic eruptions. Earth Planet. Sci. Lett. 193 (1–2), 47–56. http://dx.doi.org/10.1016/S0012-821X(01)00488-5.

Bukur, D.B., Patel, S.A., Daly, J.G., 1990. Gas holdup and solids dispersion in a three-phase slurry bubble column. AIChE J. 36, 1731–1735.
Chevrel, M.O., Cimarelli, C., DeBiasi, L., Hanson, J.B., Lavallée, Y., Arzilli, F., Dingwell, D.B., 2015. Viscosity measurements of crystallizing andesite from Tungurahua volcano (Ecuador). Geochem. Geophys. Geosyst. 16, 870–889. http://dx.doi.org/10.1002/2014GC005661.
Cimarelli, C., Costa, A., Mueller, S., Mader, H.M., 2011. Rheology of magmas with bimodal crystal size and shape distributions: insights from analog experiments. Geochem. Geophys. Geosyst. 12, Q07024. http://dx.doi.org/10.1029/2011GC003606.
Costa, A., Caricchi, L., Bagdassarov, N., 2009. A model for the rheology of particle-bearing suspensions and partially molten rocks. Geochem. Geophys. Geosyst. 10, Q03010. http://dx.doi.org/10.1029/2008GC002138.
Del Bello, E., Llewellin, E.W., Taddeucci, J., Scarlato, P., Lane, S.J., 2012. An analytical model for gas overpressure in slug-driven explosions: insights into Strombolian volcanic eruptions. J. Geophys. Res. 117, B02206. http://dx.doi.org/10.1029/2011JB008747.
Dibble, R.R., 1972. Seismic and related phenomena at active volcanoes in New Zealand, Hawaii, and Italy. PhD dissertation, Victoria University, Wellington.
Fiege, A., Holtz, F., Sarah, B.C., 2014. Bubble formation during decompression of andesitic melts. Am. Mineral. 99, 1052–1062. http://dx.doi.org/10.2138/am.2014.4719.
Folch, A., 2000. A numerical formulation to solve the ALE Navier–Stokes equations applied to the withdrawal of magma chambers. Doctoral thesis, Universitat Politècnica de Catalunya.
Girona, T., Costa, F., Newhall, C., Taisne, B., 2014. On depressurization of volcanic magma reservoirs by passive degassing. J. Geophys. Res. 119 (12), 2169–9356. http://dx.doi.org/10.1002/2014JB011368.
Hurwitz, S., Navon, O., 1994. Bubble nucleation in rhyolitic melts: experiments at high pressure, temperature, and water content. Earth Planet. Sci. Lett. 122, 267–280.
Ichihara, M., Rittel, D., Sturtevant, B., 2002. Fragmentation of a porous viscoelastic material: implications to magma fragmentation. J. Geophys. Res. 107 (B10), 2229. http://dx.doi.org/10.1029/2001JB000591.
Jeffery, G.B., 1922. The motion of ellipsoidal particles immersed in a viscous fluid. Proc. R. Soc. Lond. A 102, 161–179. http://dx.doi.org/10.1098/rspa.1922.0078.
Johnson, B.R., Glazner, A.F., 2010. Formation of K-feldspar megacrysts in granodioritic plutons by thermal cycling and late-stage textural coarsening. Contrib. Mineral. Petrol. 159 (5), 599–619.
Kantarci, N., Borak, F., Ulgen, K.O., 2005. Bubble column reactors. Process Biochem. 40, 2263–2283.
Kerekes, R.J., Soszynski, R.M., Tam Doo, P.A., 1985. The flocculation of pulp fibers. In: Transactions of 8th Fundamental Research Symposium, Oxford, England, September.
Kremers, S., Lavallée, Y., Hanson, J., Hess, K.-U., Chevrel, M.O., Wassermann, J., Dingwell, D.B., 2012. Shallow magma-mingling-driven Strombolian eruptions at Mt. Yasur volcano, Vanuatu. Geophys. Res. Lett. 39, L21304. http://dx.doi.org/10.1029/2012GL053312.
Lane, S.J., Chouet, B.A., Phillips, J.C., Dawson, P., Ryan, G.A., Hurst, E., 2001. Experimental observations of pressure oscillations and flow regimes in an analogue volcanic system. J. Geophys. Res. 106, 6461–6476.
Llewellin, E.W., Manga, M., 2005. Bubble suspension rheology and implications for conduit flow. J. Volcanol. Geotherm. Res. 143, 205–217.
Mader, H.M., Llewellin, E.W., Mueller, S.P., 2013. The rheology of two-phase magmas: a review and analysis. J. Volcanol. Geotherm. Res. 257, 135–158. http://dx.doi.org/10.1016/j.jvolgeores.2013.02.014.
Manga, M., Stone, H.A., 1994. Interactions between bubbles in magmas and lavas: effects of bubble deformation. J. Volcanol. Geotherm. Res. 63 (3–4), 267–279. http://dx.doi.org/10.1016/0377-0273(94)90079-5.
Manga, M., Castro, J., Cashman, K.V., Loewenberg, M., 1998. Rheology of bubble-bearing magmas. J. Volcanol. Geotherm. Res. 87, 15–28.
Mangan, M., 1998. Orientation distribution of microlites in obsidian. J. Volcanol. Geotherm. Res. 86 (1), 107–115. http://dx.doi.org/10.1016/S0377-0273(98)00084-5.
Marsh, B.D., 1981. On the crystallinity, probability of occurrence, and rheology of lava and magma. Contrib. Mineral. Petrol. 78 (1), 85–98.
Massol, H., Jaupart, C., 1999. The generation of gas overpressure in volcanic eruptions. Earth Planet. Sci. Lett. 166, 57–70.
Mena, P.C., Ruzicka, M.C., Rocha, F.A., Teixeira, J.A., Drahoš, J., 2005. Effect of solids on homogeneous–heterogeneous flow regime transition in bubble columns. Chem. Eng. Sci. 60, 6013–6026.
Metrich, N., Wallace, P.J., 2008. Volatile abundances in basaltic magmas and their degassing paths tracked by melt inclusions. Rev. Mineral. Geochem. 69, 363–402.
Moitra, P., Gonnermann, H.M., Houghton, B.F., Giachetti, T., 2013. Relating vesicle shapes in pyroclasts to eruption styles. Bull. Volcanol. 75, 691. http://dx.doi.org/10.1007/s00445-013-0691-8.
Mourtada-Bonnefoi, C.C., Laporte, D., 2004. Kinetics of bubble nucleation in a rhyolitic melt: an experimental study of the effect of ascent rate. Earth Planet. Sci. Lett. 218 (3–4), 521–537.
Mueller, S., Llewellin, E.W., Mader, H.M., 2010. The rheology of suspensions of solid particles. Proc. R. Soc. A 466, 1201–1228. http://dx.doi.org/10.1098/rspa.2009.0445.
Murphy, M.D., Sparks, R.S.J., Barclay, J., Carroll, M.R., Brewer, T.S., 2000. Remobilization of andesite magma by intrusion of mafic magma at the Soufriere Hills volcano, Montserrat, West Indies. J. Petrol. 41 (1), 21–42. http://dx.doi.org/10.1093/petrology/41.1.21.
Namiki, A., Manga, M., 2006. Influence of decompression rate on the expansion velocity and expansion style of bubbly fluids. J. Geophys. Res. 111, B11208. http://dx.doi.org/10.1029/2005JB004132.
Namiki, A., Manga, M., 2008. Transition between fragmentation and permeable outgassing of low viscosity magmas. J. Volcanol. Geotherm. Res. 169, 48–60.
Nguyen, C.T., Gonnermann, H.M., Chen, Y., Huber, C., Maiorano, A.A., Gouldstone, A., Dufek, J., 2013. Film drainage and the lifetime of bubbles. Geochem. Geophys. Geosyst. 14, 3616–3631. http://dx.doi.org/10.1002/ggge.20198.
Okumura, S., Nakano, T., Tsuchiyama, A., Nakamura, M., Uesugi, K., 2012. Experimental constraints on permeable gas transport in crystalline silicic magmas. Contrib. Mineral. Petrol. 164, 493–504. http://dx.doi.org/10.1007/s00410-012-0750-8.
Peck, D., 1978. Cooling and Vesiculation of Alae Lava Lake, Hawaii. U. S. Geol. Surv. Prof. Pap., vol. 935-B. 59 p.
Phillips, J.C., Lane, S.J., Lejeune, A.M., Hilton, M., 1995. Gum rosin-acetone system as an analogue to the degassing behavior of hydrated magmas. Bull. Volcanol. 57, 263–268.
Polacci, M., Baker, D.R., Bai, L., Mancini, L., 2008. Large vesicles record pathways of degassing at basaltic volcanoes. Bull. Volcanol. 70, 1023–1029. http://dx.doi.org/10.1007/s00445-007-0184-8.
Proussevitch, A.A., Sahagian, D.L., Anderson, A.T., 1993. Dynamics of diffusive bubble growth in magmas: isothermal case. J. Geophys. Res. 98 (B12), 22283–22307.
Rivalta, E., Pascal, K., Phillips, J., Bonaccorso, A., 2013. Explosive expansion of a slowly decompressed magma analogue: evidence for a delayed bubble nucleation. Geochem. Geophys. Geosyst. 14 (8), 3067–3084.
Ruzicka, M.C., 2006. On buoyancy in dispersion. Chem. Eng. Sci. 61 (8), 2437–2446. http://dx.doi.org/10.1016/j.ces.2005.11.011.
Smith, J.V., 2002. Structural analysis of flow-related textures in lavas. Earth-Sci. Rev. 57 (3–4), 279–297. http://dx.doi.org/10.1016/S0012-8252(01)00081-2.
Simakin, A.G., Armienti, P., Epel'baum, M.B., 1999. Coupled degassing and crystallization: experimental study at continuous pressure drop, with application to volcanic bombs. Bull. Volcanol. 61, 275–287.
Sparks, R.S.J., 1978. The dynamics of bubble formation and growth in magmas: a review and analysis. J. Volcanol. Geotherm. Res. 3, 1–37.
Stix, J., Phillips, J.C., 2012. An analog investigation of magma fragmentation and degassing: effects of pressure, volatile content, and decompression rate. J. Volcanol. Geotherm. Res. 211–212, 12–23.
Su, X., 2005. Gas holdup in a gas–liquid–fiber semi-batch bubble column. Retrospective Theses and Dissertations. Paper 1595.
Swanson, D.A., Duffield, W.A., Jackson, D.B., Peterson, D.W., 1979. Chronological Narrative of the 1969–71 Mauna Ulu Eruption of Kilauea Volcano, Hawaii. U. S. Geol. Surv. Prof. Pap., vol. 1056.
Tang, C., Heindel, T.J., 2005. Effect of fiber type on gas holdup in a cocurrent air–water–fiber bubble column. Chem. Eng. J. 111, 21–30.
Toramaru, A., 2006. BND (bubble number density) decompression rate meter for explosive volcanic eruptions. J. Volcanol. Geotherm. Res. 154, 303–316.
Ventura, G., De Rosa, R., Colletta, E., Mazzuoli, R., 1996. Deformation patterns in a high-viscosity lava flow inferred from the crystal preferred orientation and imbrication structures: an example from Salina (Aeolian Islands, southern Tyrrhenian Sea, Italy). Bull. Volcanol. 57, 555–562.